ChemMedChem





Reprint



Identification of Phenazine-Based MEMO1 Small-Molecule Inhibitors: Virtual Screening, Fluorescence Polarization Validation, and Inhibition of Breast Cancer Migration

Courtney L. Labrecque, [a] Cassidy N. Hilton, [a] Justin Airas, [a] Alexis Blake, [a] Kristen J. Rubenstein, [a] Carol A. Parish, *[a] and Julie A. Pollock*[a]

Phosphorylation-dependent protein-protein interactions play a significant role in biological signaling pathways; therefore, small molecules that are capable of influencing these interactions can be valuable research tools and have potential as pharmaceutical agents. MEMO1 (mediator of ErbB2-cell driven motility) is a phosphotyrosine-binding protein that interacts with a variety of protein partners and has been found to be upregulated in breast cancer patients. Herein, we report the first smallmolecule inhibitors of MEMO1 interactions identified through a virtual screening platform and validated in a competitive fluorescence polarization assay. Initial structure-activity relationships have been investigated for these phenazine-core inhibitors and the binding sites have been postulated using molecular dynamics simulations. The most potent biochemical inhibitor is capable of disrupting the large protein interface with a K_1 of 2.7 μ M. In addition, the most promising phenazine core compounds slow the migration of breast cancer cell lines in a scratch assay.

Introduction

Reversible phosphorylation is one of the most common regulatory mechanisms of protein function within a cell that enables dynamic and coordinated regulation of many aspects of cellular physiology such as cell differentiation, apoptosis, and proliferation. Normal cells are capable of maintaining the critical balance of phosphorylation whereas diseased cells, for example, cancerous cells, have abnormal phosphorylation statuses.[1] Although the phosphorylation status of a particular protein is dependent on the enzymes that add and remove the phosphate group (kinases and phosphatases, respectively), there are additional proteins that bind to phosphorylated residues to keep them in active or inactive states. These phosphorylation dependent protein-protein interactions (PPIs) contribute to highly complex signaling cascades, and inappropriate or sustained PPIs can result in many diseases including cancer. Consequently, chemical modulators of these interactions are crucial for the study of protein function in disease and have promise as therapeutics. The development of PPI inhibitors can be highly challenging due to their inherently diverse interfaces and large surface area. However, despite these obstacles, in recent years, there has been much progress in developing PPI inhibitors for interactions governed by phosphorylation; for example, inhibitors of the phosphotyrosine (pTyr)-binding Src homology 2 (SH2) domains have been developed and extensively investigated, and efforts have been made towards identifying small-molecule regulators of the phosphoserine/phosphothreonine (pSer/pThr)-binding family of 14-3-3 proteins.^[2]

MEMO1 (mediator of ErbB2-driven cell motility) has been identified as a new class of pTyr-binding proteins that is upregulated in greater that 40% of primary human breast tumors and has been correlated with poor prognosis.[3] Originally identified in complex with the activated receptor tyrosine protein kinase ErbB2, MEMO1 was linked to cell migration.[3c] In addition to interaction with ErbB2, MEMO1 has been found in complexes with estrogen receptor (ER), fibroblast growth factor receptor 1 (FGFR1), sphingosine-1-phosphate receptor 1 (S1PR1), insulin receptor substrate 1 (IRS1), insulinlike growth factor receptor (IGF1R), and cofilin, many of which play a role in tumorigenesis. [4] Knockdown of MEMO1 protein levels using small interfering RNA (siRNA) resulted in slowed breast cancer tumor xenograft growth in mice. [4b]

Previously, we examined the biophysical interaction of MEMO1 with a phosphorylated peptide corresponding to the ErbB2 tail using computational methods and fluorescence polarization; we identified five amino acid residues, Trp16, Tyr54, Asp189, Arg196, and Arg198 on MEMO1 that were essential for interaction with the ErbB2-derived peptide. [5] Here, we have expanded our work to identify small-molecule inhibitors of the interaction. First, we virtually screened targeted libraries for PPIs, kinases, and peptidomimetics and narrowed down to 128 commercially available compounds that were examined in a competitive fluorescence polarization assay for their ability to disrupt a preformed MEMO1 and ErbB2-peptide complex. Fluorescence polarization is a commonly employed technique for the screening of inhibitors of PPIs and has successfully identified multiple lead compounds for a variety of interactions. [6] This technique has advantages because it is a

Supporting information for this article is available on the WWW under https://doi.org/10.1002/cmdc.202000797

1163

[[]a] C. L. Labrecque, C. N. Hilton, J. Airas, A. Blake, K. J. Rubenstein, Prof. C. A. Parish, Prof. J. A. Pollock Department of Chemistry, University of Richmond 138 UR Drive, Richmond, VA 23173 (USA) E-mail: jpollock@richmond.edu cparish@richmond.edu



competitive binding assay and is amenable to high throughput screening. $^{\mbox{\scriptsize [7]}}$

Our lead compound exhibited a K_1 of approximately 20 μ M and contained a phenazine core structure. We performed initial structure-activity relationship (SAR) studies using an additional 22 commercially available compounds with the phenazine core identifying the most potent derivative to have a K_1 of less than 3 μ M. The best phenazine molecules were able to inhibit migration of SKBR3 and T47D breast cancer cell lines.

Results and Discussion

Computational screening

In order to identify potential small-molecule binders of MEMO1, we used a targeted virtual screening platform. We selected virtual libraries from Otava Chemicals and Life Chemicals that focused on three types of interactions: kinases (Otava Janus Kinase 2, Proto-oncogene tyrosine-protein kinase ABL1, Fibroblast growth factor receptor 1 tyrosine kinase, and Aurora B kinase; Life Chemicals Kinase and Kinase similarity), protein-protein interactions (Otava iPPI Bayesian, iPPI Tree, and SH2 domain; Life Chemicals PPI rule of four, PPI MLM, and PPI PubMed), and peptidomimetics (Otava Beta-turn peptidomimetic and Alpha-helix peptidomimetic; Life Chemicals Peptidomimetic) due to our knowledge of MEMO1 interaction with ErbB2 which is dependent on a phosphorylated tyrosine, is a large PPI, and can be recapitulated using a truncated peptide.

More than 70 000 compounds were screened using the HTVS, SP, and XP docking algorithms available in Glide, [8] with

ligands scoring in the top 10% advancing to the next, more stringently evaluated level. (More details can be found in the Experimental Section). Using this computational screen, each library returned approximately 0.1% of its total unique ligands.

Primary biochemical screening

Unfortunately, not all of the top scoring ligands from the virtual screen were readily commercially available so we purchased a subset of 128 compounds with a variety of chemical structures from Otava Chemicals and Life Chemicals. Each compound's ability to compete with the binding of a phosphorylated ErbB2 peptide to MEMO1 was assessed in a fluorescence polarization assay. Briefly, a fluorescein-labeled peptide corresponding to the ErbB2 tail was preincubated with purified MEMO1 and serial dilutions of the compounds (0-500 μM) were added; the anisotropy was measured and K_1 values calculated for each compound (Table S1 in the Supporting Information). As seen in Figure 1, four compounds were able to disrupt the interaction of MEMO1 and the ErbB2 peptide with K_1 values less than $500~\mu\text{M}.$ These results amounted to a $3\,\%$ biochemical hit rate from the 128 compounds identified from the virtual screen. We observed large variation in the K_1 values for compounds 5, 69, and 91 between experiments and attribute that to incomplete disruption of the PPI and potential non-specific binding of these molecules.[7c]

To avoid any promiscuous chemotypes that might fail in future studies, we subjected all of the tested compounds to two publicly available *in silico* filters to identify Pan-Assay INterference compoundS (PAINS).^[9] In the first screen (http://

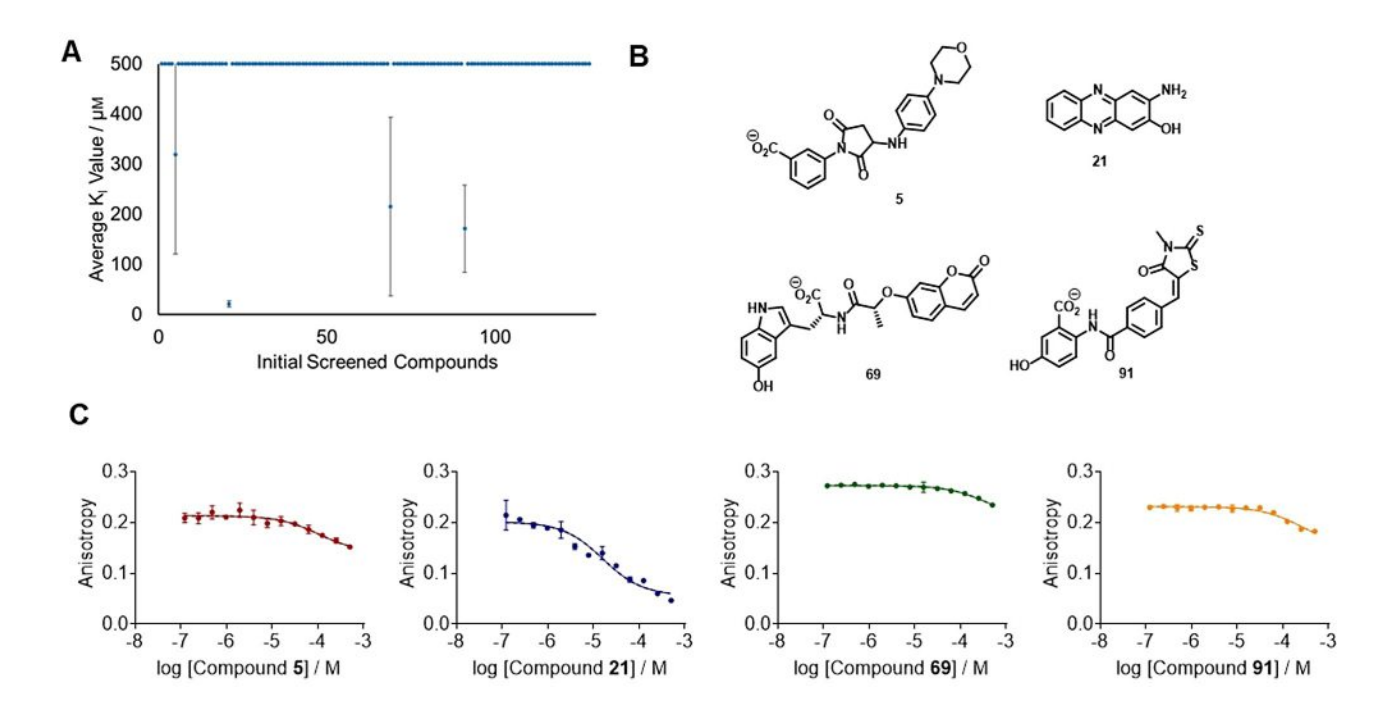


Figure 1. Initial biochemical screening of compounds. A) Results of all compounds screened in competitive fluorescence polarization assay. K_1 values presented as mean \pm standard deviation from at least three replicates. B) Structures of compounds with K_1 values less than 500 μm. C) Representative competitive isotherms for compounds with K_1 values less than 500 μm. Inhibitor concentration were diluted twofold from 500 to 0.12 μm for use in the assay.



www.cbligand.org/PAINS/), compounds **5** and **91** along with six other structures were identified as potential PAINS due to protein reactivity; they exhibited minimal inhibition in our system (Figure 1C) but were not further considered. We believe that the potential PAINS activity of compounds **5** and **91** may contribute to non-specific binding, as discussed above, resulting in the large variation in inhibition between experiments. One compound that was not a positive hit had an aggregation warning in the second screen (http://zinc15.docking.org/patterns/home/). It is not surprising that many of the screened compounds were not identified as typical PAINS because both Otava Chemicals and Life Chemicals filter their structures within the targeted libraries that we examined using similar requirements.

Of particular interest to us was compound **21**, 3-aminophenazin-2-ol, that disrupts the interaction with a K_l of $20.9\pm5.9\,\mu$ M. Interestingly, phenazine-core compounds, some of which are natural metabolites of bacteria, have been identified to have diverse biological activities including anticancer, antibiotic, antifungal, and biofilm dispersion properties. ^[10] In 2013, Gao et al. reported the synthesis of novel phenazine derivatives with apoptotic activity in a variety of cancer cell lines; the exact mechanism of action was not determined. ^[11] In addition, derivatives of 2,3-diaminophenazine were determined to slow

Table 1. MEMO1/ErbB2 interaction inhibition of substituted phenazine compounds.

N R^1 R^2								
Compound	R ¹	R ²	<i>K</i> _ι [μ м] ^[a]					
21 142 138 129 145 135 132 133 136 140	NH ₂ NH ₂ NH ₂ H CH ₃ CHO COOH CONHCy CONITOI CON(CH ₃),	OH NH ₂ H H H H H	20.9 ± 5.9 2.73 ± 0.56 151 ± 109 > 500 > 500 > 500 > 500 > 500 > 500 > 500 > 500 > 500					
149 134	NHAc NCS	NHAc H	> 500 > 500					

[a] Values are the mean \pm standard deviation of at least three separate fluorescence polarization experiments.

Table 2. MEMO1/ErbB2 interaction inhibition of charged substituted phenazine compounds.

N R2								
Compound	R ¹	R^2	$K_{\rm I} [\mu { m M}]^{\scriptscriptstyle [a]}$					
146 139 130	H CH₂CH₃ CH₂CH₂OH	H CH₂CH₃ H	119±46 >500 83.7±41.5					

[a] Values are the mean \pm standard deviation of at least three separate fluorescence polarization experiments.

lung carcinoma and colorectal cancer cell line proliferation through inhibition of human tyrosine kinase.^[12] Some literature suggest that phenazines are capable of intercalating DNA and may have general toxicity.^[13]

In order to evaluate the necessity of the phenazine core for inhibition of the MEMO1-ErbB2 peptide interaction, we purchased an additional 22 commercially available compounds containing this core from Otava Chemicals and screened them using our competitive fluorescence polarization assay. As seen in Tables 1 and 3 and S2, as well as Figure S1, eight of the 22 phenazine compounds disrupted the interaction with a $K_{\rm l}$ of less than 200 μ M; the 36% biochemical hit rate of this small library of compounds lead us to believe that this structure has promise for MEMO1 PPI inhibition. Replacement of the phenazine core with naphthalene (2,3-diaminonaphthalene and 3-amino-2-naphthol) resulted in no inhibition (Figure S2).

Initial structure-activity relationships

Although our library of phenazines is not comprehensive, we can make some initial SAR correlations. There appears to be a requirement for a hydrogen-bond participant specifically a nitrogen in the R¹ position (Table 1, compounds 21, 142, 138 vs. compound 129). In addition, a hydroxyl in the R² position is good (Table 1, compound 21) but an amine increased the activity by approximately tenfold (Table 1, compound 142). Replacement of the R² hydrogen bond participant with a hydrogen markedly decreased activity (Table 1, compound **138**). Replacement of the nitrogen in the R¹ position with an electron-withdrawing aldehyde (Table 1, compound 135), carboxylic acid (Table 1, compound 132), or amide (Table 1, compounds 133, 136, 140, 149) diminished activity altogether. Addition of an ethyl group on one of the nitrogens in the phenazine ring retained some activity if one of the hydrogens of the NH₂ was replaced with an ethanol (Table 2, compound **130**). Restricting the R¹ and R² positions into a five-membered ring such as a benzimidazole (Table 3, compounds 144 and 141) afforded very good inhibition as did the triazole (Table 3, compound 147). Replacement of amines with nitro groups or methoxy (Table S2) removed all inhibitory potential.

Table 3. MEMO1/ErbB2 interaction inhibition of benzimidazole- and triazole-substituted phenazine compounds. $\textit{K}_{\text{I}} \, [\mu \textbf{M}]^{\text{[a]}}$ R^2 Compound Х R^1 144 C Н CH₃ 9.50 ± 4.73 137 C >500 CF₃ PhOCO 141 C Н $\textbf{8.21} \pm \textbf{2.50}$ **OCOPh** PhOCO CH₂CONH₂ N/A 5.50 ± 2.69

[a] Values are the mean \pm standard deviation of at least three separate fluorescence polarization experiments.

Our previous mutagenesis and computational work^[5] suggested that MEMO1 contains at least one well-defined binding pocket that is a broad, shallow trough that extends from the vestigial binding site originally identified by Qiu et al. [14] across the backbone of the protein to a region containing residues Leu232, Lys237, His240, and Arg246 (Figure S2). In our previous studies the ErbB2-derived peptide containing a phosphorylated tyrosine was shown to bind in the vestigial pocket of the binding site by interaction with residues Trp16, Tyr54, Asp189, Arg196, and Arg198.^[5] In order to examine the SAR further, we docked the five phenazine compounds that showed the strongest experimental activities (compounds 21, 141, 142, 144, and 147; Tables 1 and 3) onto MEMO1 using Glide.[8] The top poses for four of the five compounds clustered into the same binding pocket-near the ErbB2-peptide binding site and containing Trp16, Tyr54, Asp189, Arg196, and Arg198 residues. Interestingly the top docked pose for compound 141 bound in the same site but shifted towards the other side of the binding trough. This structural shift may be due to the increased size of compound 141 relative to the other compounds and suggests that the relatively large binding cleft that runs across the face of the protein may allow both small and large ligands and proteins to bind favorably, in a variety of orientations (Figure S3). Other high scoring docked poses placed the ligands throughout the binding trough.

As a secondary screen for compound binding, we utilized differential scanning fluorimetry. $^{[5,15]}$ As seen in Table S3, compounds 21, 142, and 147 decrease the melting temperature of MEMO1 protein by 2-3 °C. Although not as common as

stabilization of protein structure, decreased stability of proteins after specific ligand binding has been observed in certain systems.^[16]

Molecular dynamics simulations

In order to develop a fuller atomistic understanding of the interaction of the phenazine compounds with MEMO1, we performed a series of computational studies to explore the specific intermolecular interactions and the overall energetics. We performed molecular dynamics (MD) simulations and MM-GBSA analysis using compounds 142, 147, and 129. In support of our biochemical results, compound 129 resulted in structural and energetic instability as well as ligand dissociation in all seeds; trajectory visualization revealed ten short-lived and unstable binding poses occurring across all seeds and no hydrogen bonds were found with an occurrence over 1%. Alternatively, compounds 142 and 147, that exhibited biochemical inhibition, showed significantly better MM-GBSA binding energies as well as long-lived binding poses with well-defined π -stacking and hydrogen bonding networks. For instance, as shown in Figure 2, the average MM-GBSA binding energy for compounds **142** and **147** was -11.86 and -18.79 kcal/mol, respectively, while the binding energy for compound 129 was -7.56 kcal/mol. During the MD simulations, compounds 142 and 147 spend considerable time in the main binding pocket, and if we filter on those frames the MM-GBSA binding energies are -15.07 and -21.40 kcal/mol, respectively. It is important to

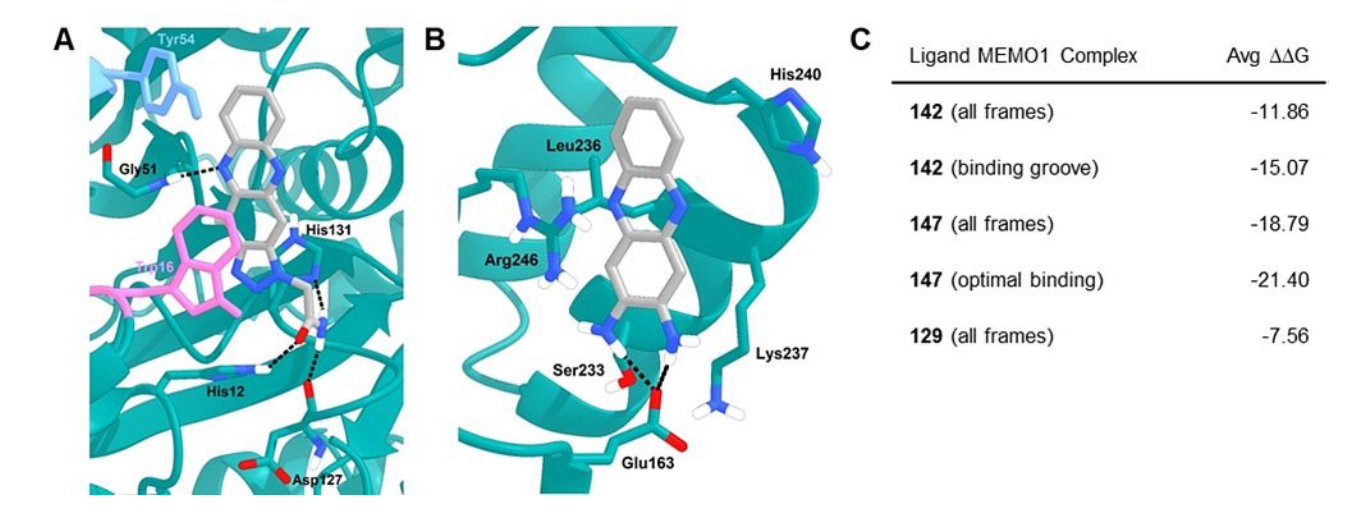


Figure 2. MEMO1 binding to phenazines. A) Compound 147 bound to the MEMO1 decamer peptide region. The most energetically favorable frame showing residues Trp16 and His131 contributing π -stacking interactions with the phenazine core of compound 147. The COM distances between these residues and compound 147 are 3.73 and 3.71 Å, respectively. The potential for π -stacking with His12 and Tyr54 is noted as well, with COM distances of 4.25 and 4.72 Å. The Gly51 backbone amine donates a hydrogen bond to the phenazine body nitrogen (25.18% occurrence in all frames sampling decamer binding-site interactions). Shorter-lived hydrogen bonds include His12 donating a hydrogen bond to the amide substituent oxygen atom (2.57%), and His131 and the Asp127 backbone accepting hydrogen bonds from the amide substituent NH₂ group (1.75 and 0.11%, respectively). Compound 147 also binds in other areas of the binding groove, as demonstrated in Figure S4. B) Compound 142 bound to the right side of the binding groove. The most energetically favorable frame showing Arg246 contributing a π -cation interaction with compound 142 (3.84 Å). Trajectory visualization suggests that His240 contributes a π -stacking interaction with compound 142 (COM distance = 5.28 Å in this frame) Hydrogen bond donation from the amine substituents to Glu163 is shown, and hydrogen bond analysis reveals that these interactions dominate this pose. In (A) and (B) all noted hydrogen bonds occur within 3 Å. Per-residue free-energy decomposition analysis supports the importance of the noted interactions. C) MMGBA energies and associated standard errors for various compounds binding to MEMO1. All energetic values are in kcal/mol.



note that the absolute values for the binding energy calculated from these methods cannot be directly compared to our experimental dissociation constants. However, the binding trends provide preliminary context for the inhibitory activity. The MD trajectories provide atomistic insight into the interactions between MEMO1 and compounds 142 and 147 (Figure 2). For instance, our MD trajectories and energetic analyses suggest that compound 142 prefers to interact with the righthand side of the binding groove (orientation relative to the image in Figure S1) forming π -cation interactions with Arg246 and possible π -stacking interactions with His240. In addition, throughout the simulation (90%), the R¹ and R² NH₂ arms are positioned for hydrogen donor interactions with Glu163. Other significant MEMO1 residue-compound 142 interactions include Ser233, Leu236, Lys237, and Asn241. When compound 147 is bound to the ErbB2-peptide binding region (left-hand side of the groove), π -stacking with Trp16 and His131 dominate the interactions, with hydrogen bonding occurring with residues His12, Gly51, and Asp127. In addition, Tyr54 is often positioned for additional π -stacking interactions. When compound 147 binds to the right-hand side of the groove, binding is weaker, and we see interactions with the same residues as for compound 142 above (Leu236, His240, Lys237, His247, Arg246). It is noteworthy that in our previous work, we saw strong interactions between the phosphorylated tyrosine in the ErbB2peptide and Trp16 and Tyr54. [5] Specific hydrogen bonding interactions and percent occurrences for compound 147 in the right side of the binding groove can be found in Figure S4.

In addition to hydrogen bonding, π -stacking is playing a significant role in the binding affinities of these phenazine-based compounds. Based on the experimental affinities shown above, and our atomistic exploration of the molecular dynamics trajectories for compounds 129, 142 and 147, it appears that the electron donating capabilities of the NH $_2$ and triazole groups on compounds 142 and 147, respectively, are increasing the electron density of the phenazine ring and correspondingly increasing the capacity for favorable π -stacking interactions with aromatic residues in MEMO1. Enhancement of the phenazine electron density is not possible with compound 129 where $R^1 = R^2 = H$, and for this compound we see significantly diminished binding (Table 1). Further evidence for the importance of phenazine substituent electronic effects and corre-

sponding π -stacking is demonstrated with the diminished binding observed when the amines of R¹ and R² are replaced with electron-withdrawing groups such as NO₂ (Table S2).

Breast cancer cellular studies

Our next step was to examine if disruption of MEMO1 interaction would result in cellular consequences. Previous studies have shown that knockdown of MEMO1 resulted in decreased migration of breast cancer cell lines including T47D, SKBR3, and MDA-MB-231 cells. [3b,c] We were able to recapitulate these results in our lab using a wound-healing assay;[17] knockdown of MEMO1 using siRNA resulted in impaired cellular migration in T47D and SKBR3 cells. Therefore, we employed this assay to evaluate phenazine compounds with the most promising biochemical inhibition (compounds 21, 130, 138, 141, 142, 144, and 147). As seen in Table 4, decreased cellular migration in comparison to the DMSO vehicle was observed in both cell lines after treatment with 100 µM compound. Some decreased wound healing could be attributed to the general or specific toxicity of the compounds as measured through a viability assay (Table 4). The compounds exhibited more toxicity in T47D cells than in SKBR3 cells; although the reasons are unknown. However, on observation of the cells after 24 hours of treatment, they did not appear to be unhealthy (Figures 3A, B, S6 and S7). Dose dependent slowed migration was observed in T47D cells for compound 142 (Figure 3C). SKBR3 and T47D cells are derived from two different kinds of breast cancer with different receptor expression levels. SKBR3 cells represent a HER2+ tumor subtype with overexpression of ErbB2 and low levels of ER and PR, while T47D cells represent a luminal A subtype with overexpression of ER and PR and low level of ErbB2.^[18] As MEMO1 has been observed to influence both ErbB2 signaling^[3c] and ER signaling,^[4f] it is consistent that our data show phenotypic activity in both cell lines. Differences between the viability and migration of the cell types could be linked to levels of MEMO1 protein or to the presence of different binding partners.

Table 4. Cellu	Table 4. Cellular consequences of treatment with phenazine compounds and their physicochemical properties.										
Compound	$EC_{50}T47D[\mu\textrm{M}]^{[a]}$	% Migration T47D ^[b]	$EC_{50} \; SKBR3 \; [\mu \textbf{m}]^{[a]}$	% Migration SKBR3 ^[c]	MW [Da]	HBD ^[d]	HBA ^[e]	$\log P^{[f]}$	log S ^[g]		
21	95±30	62±18	67 ± 15	43 ± 15	211.23	2.5	3.75	1.187	-2.37		
130	161 ± 12	47 ± 14	337 ± 60	39 ± 19	269.35	3	3.75	2.806	-3.73		
138	69 ± 20	41 ± 14	>500	34 ± 17	195.22	1.5	3	1.851	-2.62		
141	> 500	37 ± 17	>500	50 ± 23	664.67	0	11.25	5.877	-7.32		
142	46 ± 13	24 ± 14	>500	44 ± 22	210.24	3	4	1.022	-2.32		
144	33 ± 8	74 ± 23	>500	35 ± 27	234.26	1	3.5	2.465	-3.75		
147	39 ± 12	69 ± 35	>500	42 ± 23	278.27	2	6.5	0.237	-1.66		
0.2% DMSO	_	86 ± 15	_	64 ± 13	_	_	_	_	_		

[a] Cell viability after 24 h of compound treatment. Data represent mean \pm standard deviation of three experiments. [b] Percentage of relative cellular wound closure after treatment for 24 h with 100 μ M of the indicated compounds. Data represent mean \pm standard deviation of four experiments. Representative images can be found in Figures 3A, B and S6. [c] Percentage of relative cellular wound closure after treatment for 48 h with 100 μ M of the indicated compounds. Data represent mean \pm standard deviation of four experiments. Representative images can be found in Figure S7. [d] Number of hydrogen bond donors. [e] Number of hydrogen bond acceptors. [f] The predicted octanol/water partition coefficient. [g] The predicted aqueous solubility.

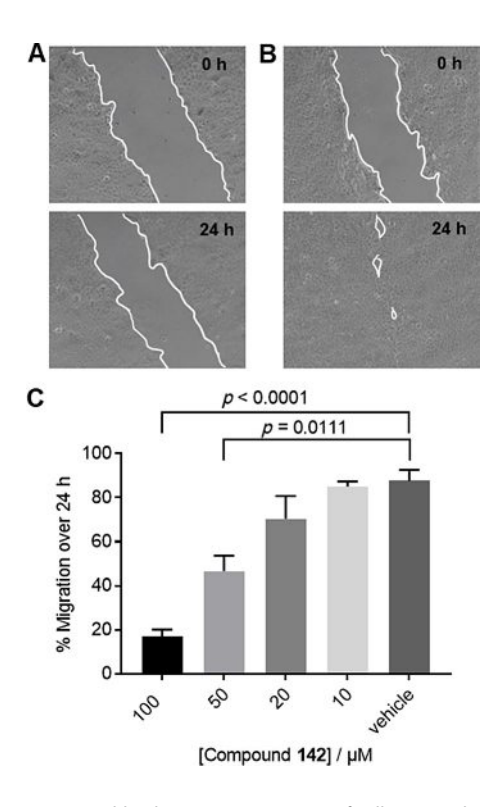


Figure 3. T47D wound-healing assay. A) Images of cells at 0 and 24 h after treatment with 100 μM of compound **142**. B) Images of vehicle-treated (0.2% DMSO) cells at 0 and 24 h. C) Migration of cells over 24 h at the indicated concentrations of compound **142**. Data represents mean \pm standard error mean of four experiments. Statistical differences were calculated with the Student t test versus vehicle treated cells.

Conclusions

Previously, we developed a fluorescence polarization assay for the characterization of MEMO1 and peptide-binding partners. [5] Here, we have expanded the utility of the fluorescence polarization assay to biochemically identify small-molecule inhibitors of the MEMO1-ErbB2 derived peptide interaction. Beginning with a virtual screening platform, we identified a core phenazine structure with inhibitory potential. Through limited SAR, we have determined the necessity of appended electrondonating groups on the phenazine core with the ability to form productive hydrogen bond and $\pi\text{-stacking}$ interactions with MEMO1. Interestingly, our MD simulations of two phenazine inhibitors provide two distinct potential binding sites within the MEMO1-protein interaction trough. More detailed molecular studies will reveal the exact binding mode and could contribute to the design of more potent inhibitors. The inhibitory activity of our best compounds (2-8 µM) is modest; however, they provide a starting point for additional optimization. PPIs are typically difficult to target with small molecules and initial screening efforts, similar to ours, have provided lead compounds with comparable potencies. [19]

To our knowledge, these compounds are the first small molecules targeting the MEMO1 PPI interface. They will be invaluable tools for investigating the role of MEMO1 in biological contexts. Indeed, we observe that similar to MEMO1

knockdown in breast cancer cell lines, the phenazine compounds slow cellular migration in a scratch assay.

The importance of MEMO1 as a scaffolding protein for phosphorylation-dependent protein-protein interactions within breast cancer is clear; however, its role in other biological processes is continuing to be discovered. For example, high levels of MEMO1 have been correlated with colorectal cancer, and its function has been linked to neuroinflammation and neuronal development.^[20] In addition to the protein scaffolding function, MEMO1 has been shown to be a redox protein and has been linked to metal homeostasis and consequently conditions such as premature aging, kidney disease, and bone demineralization.^[21] All previous studies have utilized genetic manipulation and knockdown experimentation to investigate MEMO1 function. The phenazine compounds identified here will provide additional tools for manipulation of MEMO1 activity.

Experimental Section

General information

The chemical databases used for the virtual screening were obtained from LifeChemicals and Otava Chemicals. Compounds identified from the virtual screening as potential inhibitors that were commercially and readily available were purchased from the respective companies. 2,3-diaminonaphthalene was purchased from Oakwood chemicals and 3-amino-2-naphthol was purchased from VWR. The N-terminal fluorescein labeled-peptide corresponding to the ErbB2 tail (1217Phe-Asp-Asn-Leu-Tyr-pTyr-Trp-Asp-Gln-Asp1226-NH₂, FL-pYD10) used for fluorescence polarization studies was custom synthesized by Genscript. Recombinant MEMO1 used in the fluorescence polarization assay was prepared as described previously.^[5] All statistical analysis and graphing was carried out in GraphPad Prism 8.

Computational studies

Ligand retrieval and preparation: Three-dimensional ligand structures were obtained from structure data files (SDF) provided by LifeChemicals and Otava Chemicals. Schrodinger's LigPrep was used to optimize ligand structures. Within LigPrep, Epik $^{[22]}$ was used to produce all possible ligand protonation states at a pH of 7 ± 2 . All ligands were desalted, and possible tautomers were sampled. Additionally, up to 32 stereoisomers were generated for each ligand, and the specified chiralities of each molecule were retained.

Protein retrieval and preparation: The crystal structure of MEMO1 was obtained from the Protein Data Bank (PDB ID: 3BCZ). Chain A was selected, and its glycerol ligand was removed. Schrödinger's Protein Preparation Wizard^[23] was used to optimize the protein. These optimizations include the conversion of selenomethionine residues in the experimental structure to methionine residues, as well as the assignment of bond orders using the CCD database and the addition of missing hydrogen atoms. Prediction of likely side chain protonation states within a pH range of 7 ± 2 was conducted using Epik. Hydrogen bonds were optimized while sampling water orientations using PROPKA at a pH of 7, and restrained minimization was then performed using the OPLS3 force field. [24]

SiteMap and receptor grid generation: Schrödinger's SiteMap program^[19] was used to predict and score potential ligand binding



sites. Potential binding sites are assigned separate Site Scores (Sscore) and Drugability Scores (Dscore) based on properties such as the volume, hydrophobicity, hydrophilicity, and H-bonding ability of the site. Binding sites with a Sscore of at least 0.8 and a Dscore of at least 0.83 are likely to allow ligand binding to occur. [25] With all parameters set to default, three potential binding sites were identified. One of these sites (Site #1) returned scores suggestive of good binding. Schrödinger's Receptor Grid Generation was then used to generate a 30×40×20 Å receptor grid encompassing this binding site. A ligand size cutoff of 20 Å was applied. All other parameters were kept at their default values. The resultant receptor grid was used for all subsequent ligand docking.

Ligand docking: Using Schrödinger's Glide Docking program, [26] each prepared ligand library was docked into the binding site encompassed by the receptor grid. Glide assigns a GlideScore to each ligand based on their predicted polar and nonpolar interactions within the receptor grid. Default parameters were used in conjunction with the HTVS, SP, and XP docking algorithms in a successive fashion. These algorithms score each ligand based on its predicted chemical interactions within the specified binding site. While HTVS will dock any ligand that may reasonably be expected to bind, XP more stringently considers hydrogen bonding and the hydrophobic enclosure of lipophilic ligand atoms. After each docking round, ligands scoring in the top 10% were then run through the next, more stringent algorithm.

Molecular dynamics simulations with AMBER18: AMBER Unrestrained Molecular Dynamics^[27] simulations were used to study the dynamics of the ligand-protein complex. Initial structures were taken from the top scoring Glide pose for compounds 129, 142, and 147 docked to MEMO1. To diversify the set of initial structures, we also utilized lower scoring Glide poses still within the binding groove. The ff14SB force field^[28] was applied to the protein. The GAFF force field and AM1-BCC charges were applied to all ligands using antechamber. All models were explicitly solvated in a unit cell with TIP3P water molecules^[29] and neutralized with CI⁻ and Na⁺ ions using tleap. The AMBER18 GPU-accelerated pmemd code was used to run all simulations.[30] Each ligand-protein complex was minimized, heated, equilibrated, and subjected to unrestrained MD simulations. All structures were subjected to a seven-step minimization process involving 1000 steps of the steepest descent minimization followed by 4000 steps of conjugate gradient minimization. This minimization approach optimized the structure and reduced the possibility of clashes created by hydrogen atoms, ions, and/ water molecules. A 12.0 Å cutoff was used so that only non-bonded atoms within a 12.0 Å radius could contribute to the non-bonded energy term of a specific atom. A restraint weight of 10.0 kcal/mol/Å was used on all non-hydrogen atoms in the system. This restraint was successfully lowered over seven steps of minimization (5.0 \rightarrow 2.0 \rightarrow 1.0 \rightarrow 0.5 \rightarrow 0.1 \rightarrow 0.0 kcal/mol/Å) until the restraints were removed altogether and the atoms were allowed to minimize freely. After minimization, each molecular system was heated and assigned a random initial velocity. During heating, the system started at step 0 at a temperature of 10.0 K and increased linearly until it reached 300 K. After the solvent reached the target temperature, the solute was equilibrated within the system. During the seven stages of equilibration, the restraint was slowly reduced every 500 ps. The restraint weight during equilibration is lowered identically to the restraint weight during the minimization step. Upon completion of the equilibration, unrestrained molecular dynamics was performed on each system for 1000 ns using four different, randomly selected seeds (initial velocities). Dynamical information was obtained from the MD trajectories using cpptraj. RMSD values from the initial structure and hydrogen bonding analysis provided information about conformational flexibility and important intra- and inter-molecular interactions. Binding free energies were computed every 0.1 ns using MM-GBSA. $^{[31]}$ Trajectory visualization was conducted using UCSF Chimera. $^{[32]}$

Calculation of physicochemical properties: Octanol/water partition coefficients and predicted solubilities, along with molecular properties such as molecular weight, and number of hydrogen bond donors and acceptors were calculated using Schrodinger's QikProp program. These and other absorption, distribution, metabolism and excretion (ADME) values were used to evaluate the suitability of our highest scoring drug candidates.

Biological evaluation

Fluorescence polarization competitive assay: Twofold serial dilutions of the compounds (0-500 μM) were made in sodium phosphate buffer (50 mM, pH 6.4). MEMO1 and labeled phosphorylated peptide (FL-pYD10) were mixed in a separate tube along with sodium phosphate buffer and incubated at room temperature for 10 min. The preformed MEMO1 and FL-pYD10 complex was added to the serial dilutions of the compounds to a final concentration of 2.5 μM MEMO1 and 50 nM FL-pYD10. The combined mixture of compound, MEMO1, and FL-pYD10 was incubated for an additional 10 min at room temperature. Each dilution was pipetted in triplicate into a black 384-well plate (20 µL to each well). 1 % DMSO solution served as the plate blank. All samples were plated and spun down at 58 x g for 30 s. Fluorescence measurements were taken using a SpectraMax i3 plate reader (Molecular Devices) with a fixed excitation (485 nm) and emission (525 nm). The Z' factor was calculated for each compound based on the following equation (σ_b and $\sigma_{\!\scriptscriptstyle f}$ are the standard deviations of the emission anisotropy for the bound and free probe, respectively, and U_b and U_f are the means of the emission anisotropy of the bound and free probes, respectively):[7a]

$$Z' = 1 - \frac{3\sigma_b + 3\sigma_f}{U_b - U_f} \tag{1}$$

All Z^\prime values were found to be between 0.70 and 0.91, indicating excellent assay performance.

Millipolarization (mP) was calculated using the Softmax Pro software from parallel and perpendicular intensities ($Q_{\rm para}$ and $Q_{\rm perp}$ respectively). The G factor was determined as described previously to be 1.4.^[5]

$$mP = 1000 \times \frac{Q_{\text{para}} - GQ_{\text{perp}}}{Q_{\text{para}} + GQ_{\text{perp}}}$$
 (2)

mP was subsequently converted to units of anisotropy (A):

$$A = \frac{2\left(\frac{mP}{1000}\right)}{3 - \frac{mP}{1000}} \tag{3}$$

The K_1 for each compound was determined from the fit (EC₅₀) of the anisotropy vs. log[inhibitor] curve and the concentration (50 nM) and K_D (532 nM) of FL-pYD10 using GraphPad Prism 8:

$$logEC_{50} = log \left(10^{logK_{I}^{*}\left(1 + \frac{50}{532} \frac{nM}{nM}\right)}\right)$$
 (4)

Background anisotropy of compounds **21**, **129–150** was measured in the presence of 50 nM FL-pYD10 (Figure S7).



Protein thermal stability by differential scanning fluorimetry. As previously described, [5,15] purified protein (0.3 mg/mL), compound (50 μ M), and SYPRO Orange protein stain (1:500 relative dilution) were combined to a final volume of 100 μ L. Each sample was loaded in triplicate into a 96-well, clear PCR plate (25 μ L per well), and the plate was sealed. The samples were then heated from 15 to 95 °C at a rate of 0.5 °C/min in a Bio-Rad RT-PCR machine. SYPRO Orange fluorescence was monitored, and the midpoint of the plot of the first derivative of fluorescence versus temperature was used to determine the melting temperature ($T_{\rm m}$).

Cell culture: SKBR3 and T47D cell lines were obtained from the American Type Culture Collection (ATCC). SKBR3 cells were cultured in McCoy's 5 A medium (GenClone) containing L-glutamine and sodium bicarbonate, while T47D cells were cultured in RPMI-1640 medium (GenClone) containing L-glutamine. Both types of media were supplemented with heat-inactivated 10% fetal Bovine Serum (Invitrogen), 100 U/mL Penicillin and 100 μg/mL streptomycin (GenClone). Cells were grown at 37 °C under 5% CO₂.

Cell viability assay: SKBR3 and T47D cells were seeded at 5000 cells per well in a 96-well plates in growth medium. After 2–4 days, the cells were given fresh media and treated with the inhibitors at various concentrations (3.9–500 $\mu\text{M})$ or control (0.2% DMSO) for 24 h at 37 °C. Cells were incubated for 2 h at 37 °C after addition of 0.15 mg/mL resazurin in PBS (pH 7.4). Fluorescence was subsequently measured ($\lambda_{\text{ex}}{=}570$ nm, $\lambda_{\text{em}}{=}585$ nm) using a SpectroMax i3 plate reader (Molecular Devices). The data were background corrected using a "no cell" control.

Wound-healing migration assay: The general procedure from Liang, et. al. was followed. [17b] Briefly, SKBR3 or T47D cells were seeded to 90% confluence in a 24-well plate. The cells were scratched with a p10 micropipette tip, rinsed with 1x PBS (pH 7.4), and treated with 500 μL compound-containing medium or 500 μL control medium with 0.2% DMSO. The compound-containing media was prepared by diluting each compound to the indicated final concentrations in the respective growth media. For knockdown experiments, siRNA for MEMO1 was purchased from Origene and transfected into the cells using Lipofectamine 3000 (Invitrogen) following the manufacturer's protocol. Photographs of the scratch were captured at 0, 1, 4, 8, 12, 24, and 48 h time points at the same location for each well. Growth media and DMSO diluted in growth media were used as controls. The photographs were analyzed using the NIS-elements D ver. 5.11 software to measure the area not covered by cells.

Acknowledgements

This research was supported by funding from the Virginia Academy of Sciences Mary Louise Andrews Award for Cancer Research; The Thomas F. and Kate Miller Jeffress Memorial Trust, Bank of America, Trustee; the National Science Foundation (Grant CHE-1800014 to C.A.P.); the Floyd D. and Elisabeth S. Gottwald Foundation (C.A.P.); and start-up funds from the University of Richmond (J.A.P.). A.B. was the recipient of a post-baccalaureate fellowship from the University of Richmond Integrated and Inclusive Science program. C.L.L., C.N.H., and J.A. were recipients of summer fellowships from the Puryear-Topham-Pierce endowment from the Department of Chemistry at the University of Richmond. A.B. and J.A. were recipients of summer fellowships from the University of Richmond Arts and Sciences Undergraduate Research Committee.

Conflict of Interest

The authors declare no conflict of interest.

Keywords: breast cancer \cdot MEMO1 \cdot migration \cdot phenazine \cdot protein-protein interactions

- [1] P. Cohen, Eur. J. Biochem. 2001, 268, 5001-5010.
- [2] a) X. Ran, J. E. Gestwicki, Curr. Opin. Chem. Biol. 2018, 44, 75–86; b) W. C. Shakespeare, Curr. Opin. Chem. Biol. 2001, 5, 409–415; c) P. Thiel, L. Roglin, N. Meissner, S. Hennig, O. Kohlbacher, C. Ottmann, Chem. Commun. 2013, 49, 8468–8470; d) N. Watanabe, H. Osada, Bioorg. Med. Chem. 2016, 24, 3246–3254; e) H. Wu, J. Ge, S. Q. Yao, Angew. Chem. 2010, 49, 6528–6532. f) M. Mori, G. Vignaroli, Y. Cau, J. Dinic, R. Hill, M. Rossi, D. Colecchia, M. Pesic, W. Link, M. Chiariello, C. Ottmann, M. Botta, ChemMedChem 2014, 9, 973–983.
- [3] a) M. Feracci, C. Pimentel, O. Bornet, P. Roche, D. Salaun, A. Badache, F. Guerlesquin, FEBS Lett. 2011, 585, 2688–2692; b) G. MacDonald, I. Nalvarte, T. Smirnova, M. Vecchi, N. Aceto, A. Doelemeyer, A. Frei, S. Lienhard, J. Wyckoff, D. Hess, J. Seebacher, J. J. Keusch, H. Gut, D. Salaun, G. Mazzarol, D. Disalvatore, M. Bentires-Alj, P. P. Di Fiore, A. Badache, N. E. Hynes, Sci. Signaling 2014, 7; c) R. Marone, D. Hess, D. Dankort, W. J. Muller, N. E. Hynes, A. Badache, Nature Cell Biol. 2004, 6, 515–522.
- [4] a) B. Haenzi, O. Bonny, R. Masson, S. Lienhard, J. H. Dey, M. Kuro-o, N. E. Hynes, FASEB J. 2014, 28, 327–336; b) K. Jiang, Z. Yang, L. Cheng, S. Wang, K. Ning, L. Zhou, J. Lin, H. Zhong, L. Wang, Y. Li, J. Huang, H. Zhang, Q. Ye, J. Biol. Chem. 2013, 288, 24590–24599; c) S. Kondo, A. Bottos, J. C. Allegood, R. Masson, F. G. Maurer, C. Genoud, P. Kaeser, A. Huwiler, M. Murakami, S. Spiegel, N. E. Hynes, PLoS One 2014, 9; d) M. Meira, R. Masson, I. Stagljar, S. Lienhard, F. Maurer, A. Boulay, N. E. Hynes, J. Cell Sci. 2009, 122, 787–797; e) A. V. Sorokin, J. Chen, Oncogene 2013, 32, 3130–3138; f) A. Frei, G. MacDonald, I. Lund, J. A. Gustafsson, N. E. Hynes, I. Nalvarte, Oncotarget 2016, 7, 56170-56182.
- [5] M. L. Newkirk, K. J. Rubenstein, J. Y. Kim, C. L. Labrecque, J. Airas, C. A. Taylor, H. D. Evans, Q. McKoy, C. A. Parish, J. A. Pollock, *Biochemistry* 2018, 57, 5169–5181.
- [6] a) A. M. Beekman, M. A. O'Connell, L. A. Howell, ChemMedChem 2016, 11, 840–844; b) R. C. Dash, Z. Ozen, K. R. McCarthy, N. Chatterjee, C. A. Harris, A. A. Rizzo, G. C. Walker, D. M. Korzhnev, M. K. Hadden, Chem-MedChem 2019, 14, 1610–1617; c) P. Hu, X. Wang, B. Zhang, S. Zhang, Q. Wang, Z. Wang, ChemMedChem 2014, 9, 928–931; d) T. Mani, D. Liu, D. Zhou, L. Li, W. E. Knabe, F. Wang, K. Oh, S. O. Meroueh, ChemMedChem 2013, 8, 1963–1977; e) W. Reindl, M. Graber, K. Strebhardt, T. Berg, Anal. Biochem. 2009, 395, 189–194; f) M. H. Roehrl, J. Y. Wang, G. Wagner, Biochemistry 2004, 43, 16067–16075; g) H. M. Shan, Y. Shi, J. Quan, ChemMedChem 2015, 10, 158–163
- [7] a) M. D. Hall, A. Yasgar, T. Peryea, J. C. Braisted, A. Jadhav, A. Simeonov, N. P. Coussens, *Methods Appl. Fluoresc.* 2016, 4, 022001. b) W. A. Lea, A. Simeonov, Ex. Opin. Drug Dis. 2011, 6, 17–32. c) M. H. Roehrl, J. Y. Wang, G. Wagner, *Biochemistry* 2004, 43, 16056–16066. d) A. Ciulli, *Methods Mol. Biol.* 2013, 1008, 357–388.
- [8] a) R. A. Friesner, J. L. Banks, R. B. Murphy, J. Med. Chem. 2004, 1739–1749; b) R. A. Friesner, R. B. Murphy, M. P. Repasky, J. Med. Chem. 2006, 6177–6196; c) T. A. Halgren, R. B. Murphy, R. A. Friesner, J. Med. Chem. 2004, 1750–1759.
- [9] J. B. Baell, G. A. Holloway, J. Med. Chem. 2010, 53, 2719–2740.
- [10] a) N. Guttenberger, W. Blankenfeldt, R. Breinbauer, Bioorg. Med. Chem. 2017, 25, 6149–6166; b) M.-Z. Wang, H. Xu, S.-J. Yu, Q. Feng, S.-H. Wang, Z.-M. Li, J. Agric. Food Chem. 2010, 58, 3651–3660.
- [11] X. Gao, Y. Lu, L. Fang, X. Fang, Y. Xing, S. Gou, T. Xi, Eur. J. Med. Chem. 2013, 69, 1–9.
- [12] A. M. Mahran, S. Ragab, A. I. Hashem, M. M. Ali, A. A. Nada, Eur. J. Med. Chem. 2015, 90, 568–576.
- [13] G. W. Rewcastle, W. A. Denny, B. C. Baguley, J. Med. Chem. 1987, 30, 843–851.
- [14] C. Qiu, S. Lienhard, N. E. Hynes, A. Badache, D. J. Leahy, J. Biol. Chem. 2008, 283, 2734–2740.
- [15] J. J. Lavinder, S. B. Hari, B. J. Sullivan, T. J. Magliery, J. Am. Chem. Soc. 2009, 131, 3794–3795.



- [16] a) P. Cimmperman, L. Baranauskiene, S. Jachimoviciute, J. Jachno, J. Torresan, V. Michailoviene, J. Matuliene, J. Sereikaite, V. Bumelis, D. Matulis, Biophys. J. 2008, 95, 3222–3231; b) C. Hamiaux, R. S. Drummond, B. J. Janssen, S. E. Ledger, J. M. Cooney, R. D. Newcomb, K. C. Snowden, Curr. Biol. 2012, 22, 2032–2036; c) M. E. Pacold, K. R. Brimacombe, S. H. Chan, J. M. Rohde, C. A. Lewis, L. J. Swier, R. Possemato, W. W. Chen, L. B. Sullivan, B. P. Fiske, S. Cho, E. Freinkman, K. Birsoy, M. Abu-Remaileh, Y. D. Shaul, C. M. Liu, M. Zhou, M. J. Koh, H. Chung, S. M. Davidson, A. Luengo, A. Q. Wang, X. Xu, A. Yasgar, L. Liu, G. Rai, K. D. Westover, M. G. Vander Heiden, M. Shen, N. S. Gray, M. B. Boxer, D. M. Sabatini, Nat. Chem. Biol. 2016, 12, 452–458.
- [17] a) C. Jadala, M. Sathish, P. Anchi, R. Tokala, U. J. Lakshmi, V. G. Reddy, N. Shankaraiah, C. Godugu, A. Kamal, *ChemMedChem* 2019, 14, 2052–2060; b) C. C. Liang, A. Y. Park, J. L. Guan, *Nature Prot.* 2007, 2, 329–333.
- [18] X. Dai, H. Cheng, Z. Bai, J. Li, J. Cancer 2017, 8, 3131–3141.
- [19] a) U. Švajger, B. Brus, S. Turk, M. Sova, V. Hodnik, G. Anderluh, S. Gobec, Eur. J. Med. Chem. 2013, 70, 393–399; b) M. Vincendeau, K. Hadian, A. C. Messias, J. K. Brenke, J. Halander, R. Griesbach, U. Greczmiel, A. Bertossi, R. Stehle, D. Nagel, K. Demski, H. Velvarska, D. Niessing, A. Geerlof, M. Sattler, D. Krappmann, Sci. Rep. 2016, 6, 18934.
- [20] a) V. Bogoevska, G. Wolters-Eisfeld, B. T. Hofmann, A. T. El Gammal, B. Mercanoglu, F. Gebauer, Y. K. Vashist, D. Bogoevski, D. Perez, N. Gagliani, J. R. Izbicki, M. Bockhorn, C. Gungor, Oncogene 2017, 36, 2394–2404; b) N. Nakagawa, C. Plestant, K. Yabuno-Nakagawa, J. Li, J. Lee, C. W. Huang, A. Lee, O. Krupa, A. Adhikari, S. Thompson, T. Rhynes, V. Arevalo, J. L. Stein, Z. Molnar, A. Badache, E. S. Anton, Neuron 2019, 103, 836–852 e835; c) S. Sarkar, E. B. Dammer, E. Malovic, A. L. Olsen, S. A. Raza, T. Gao, H. Xiao, D. L. Oliver, D. Duong, V. Joers, N. Seyfried, M. Huang, T. Kukar, M. G. Tansey, A. G. Kanthasamy, S. Rangaraju, Front. Immunol. 2020, 11, 33.
- [21] a) M. B. Moor, B. Haenzi, F. Legrand, R. Koesters, N. E. Hynes, O. Bonny, Frontiers Physiol. 2018, 9, 874; b) M. B. Moor, S. K. Ramakrishnan, F. Legrand, M. Bachtler, R. Koesters, N. E. Hynes, A. Pasch, O. Bonny, PLoS One 2020, 15, e0236361; c) M. B. Moor, S. K. Ramakrishnan, F. Legrand, S. Dolder, M. Siegrist, F. Durussel, G. Centeno, D. Firsov, N. E. Hynes, W. Hofstetter, O. Bonny, JBMR Plus 2018, 2, 195–205.
- [22] J. R. Greenwood, D. Calkins, A. P. Sullivan, J. C. Shelley, J. Comput.-Aided Mol. Des. 2010, 24, 591–604.
- [23] G. Madhavi Sastry, M. Adzhigirey, T. Day, R. Annabhimoju, W. Sherman, J. Comput.-Aided Mol. Des. 2013, 27, 221–234.
- [24] E. Harder, W. Damm, J. Maple, C. Wu, M. Reboul, J. Y. Xiang, L. Wang, D. Lupyan, M. K. Dahlgren, J. L. Knight, J. W. Kaus, D. S. Cerutti, G. Krilov,

- W. L. Jorgensen, R. Abel, R. A. Friesner, J. Chem. Theory Comput. 2016, 12, 281–296.
- [25] a) T. A. Halgren, J. Chem. Inf. Model. 2009, 49, 377–389. b) T. Halgren, Chem. Biol. Drug Des. 2007, 69, 146–148.
- [26] a) R. A. Friesner, R. B. Murphy, M. P. Repasky, L. L. Frye, J. R. Greenwood, T. A. Halgren, P. C. Sanschagrin, D. T. Mainz, J. Med. Chem. 2006, 49, 6177–6196; b) T. A. Halgren, R. B. Murphy, R. A. Friesner, H. S. Beard, L. L. Frye, W. T. Pollard, J. L. Banks, J. Med. Chem. 2004, 47, 1750–1759; c) R. A. Friesner, J. L. Banks, R. B. Murphy, T. A. Halgren, J. J. Klicic, D. T. Mainz, M. P. Repasky, E. H. Knoll, M. Shelley, J. K. Perry, D. E. Shaw, P. Francis, P. S. Shenkin, J. Med. Chem. 2004, 47, 1739–1749.
- 27] D. A. Case, K. Belfon, I. Y. Ben-Shalom, S. R. Brozell, D. S. Cerutti, I. T. E. Cheatham, V. W. D. Cruzeiro, T. A. Darden, R. E. Duke, G. Giambasu, M. K. Gilson, H. Gohlke, A. W. Goetz, R. Harris, S. Izadi, K. K. Jhala, A. Kovalenko, R. Krasny, T. Kurtzman, T. S. Lee, S. LeGrand, P. Li, C. Lin, J. Liu, T. Luchko, R. Luo, V. Man, K. M. Merz, Y. Miao, O. Mikhailovskii, G. Monard, H. Nguyen, A. Onufriev, F. Pan, S. Pantano, R. Qi, D. R. Roe, A. Roitberg, C. Sagui, S. Schott-Verdugo, J. Shen, C. L. Simmerling, N. Skrynnikov, J. Smith, J. Swails, R. C. Walker, J. Wang, L. Wilson, R. M. Wolf, X. Wu, D. M. York, P. A. Kollman, AMBER18, University of California, San Francisco, 2018.
- [28] J. A. Maier, C. Martinez, K. Kasavajhala, L. Wickstrom, K. E. Hauser, C. Simmerling, J. Chem. Theory Comput. 2015, 11, 3696–3713.
- [29] P. Mark, L. Nilsson, J. Phys. Chem. A 2001, 105, 9954–9960.
- [30] a) A. W. Götz, M. J. Williamson, D. Xu, D. Poole, S. Le Grand, R. C. Walker, J. Chem. Theory Comput. 2012, 8, 1542–1555; b) R. Salomon-Ferrer, A. W. Götz, D. Poole, S. Le Grand, R. C. Walker, J. Chem. Theory Comput. 2013, 9, 3878–3888.
- [31] B. R. Miller, T. D. McGee, J. M. Swails, N. Homeyer, H. Gohlke, A. E. Roitberg, J. Chem. Theory Comput. 2012, 8, 3314–3321.
- [32] E. F. Pettersen, T. D. Goddard, C. C. Huang, G. S. Couch, D. M. Greenblatt, E. C. Meng, T. E. Ferrin, J. Comput. Chem. 2004, 25, 1605–1612.
- [33] Schrodinger Release 2016–4: QikProp, Schrodinger, LLC, New York, NY, 2020.

Manuscript received: October 13, 2020 Revised manuscript received: December 15, 2020 Accepted manuscript online: December 17, 2020 Version of record online: January 26, 2021